Electronic Supplementary Material (ESI) for New Journal of Chemistry.
This journal is © The Royal Society of Chemistry and the Centre National de la Recherche Scientifique 2017

Three-dimensional flower-like $Mg(OH)_2$@MoS_2 nanocomposite: fabrication, characterization and high-performance sensing properties to NO_x at room temperature

Jiameng Kang[a], Muhammad Ikram[a], Yiming Zhao [a], Jiawei Zhang[b]*, Afrasiab Ur Rehman[a], Lihong Gong[b], Keying Shi[a]*

[a] *Key Laboratory of Functional Inorganic Material Chemistry, Ministry of Education. School of Chemistry and Material Science, Heilongjiang University, Harbin, 150080, P. R. China.*

[b]*Key Laboratory for Photonic and Electronic, Ministry of Education. Modern experiment center, Harbin Normal University, Harbin 150025, P. R. China.*

Corresponding author. Tel.: +86 451 86609141; +86 451 86604920

E-mail: jiaweizhang1@163.com, shikeying2008@163.com

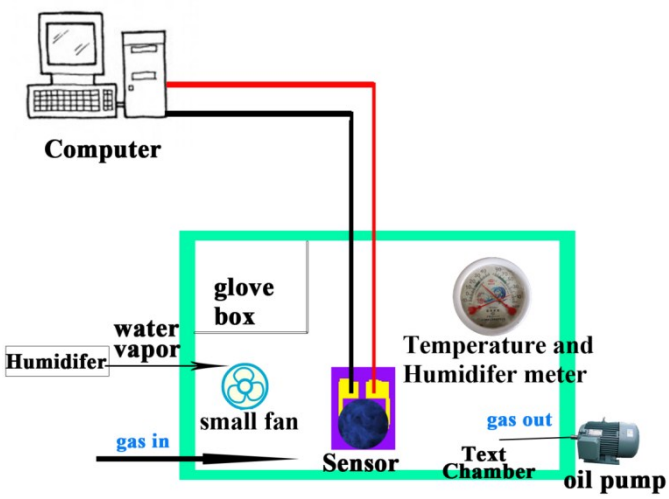

Fig. S1 The diagram of the sensor detection for the gas sensing process.

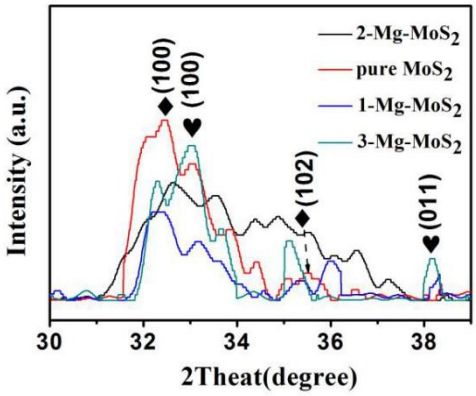

Fig. S2A XRD patterns of the pure MoS_2, 1-Mg-MoS_2, 2-Mg-MoS_2 and 3-Mg-MoS_2.

With the increase of $Mg(OH)_2$ content, the peak of MoS_2 (100) (2-Mg-MoS_2) broaden significantly, and the peak of MoS_2 (100) combined with the peak (011) of $Mg(OH)_2$ (see Fig.S2). Comparison with pure MoS_2, the MoS_2 (100) and (102) peaks of 2-Mg-MoS_2 sample shifted to small angle, this might result from the insertion of a small amount of Mg^{2+} ions in the MoS_2 interlayer during the hydrothermal process (Mo^{4+} ion radius was 0.065 nm; Mg^{2+} ion radius was 0.072 nm) [1], which could modify the electronic state of MoS_2.

Furthermore, the isomorphic substitution of high valence Mo^{4+} ions will result in more defects.

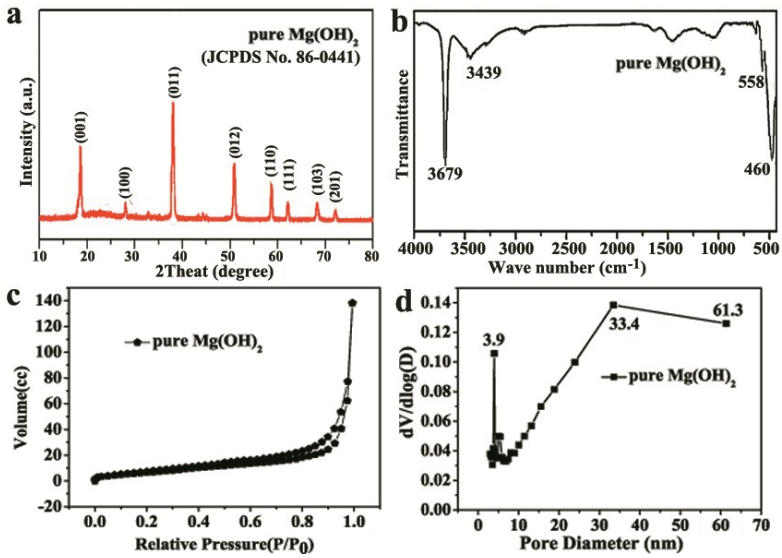

Fig. S2B. Pure $Mg(OH)_2$ of (a) XRD diffraction pattern; (b) FT-IR spectrum; (c) N_2 adsorption-desorption isotherm; and (d) The pore diameter distribution curve.

Table S1 The Characteristic peaks of FT-IR spectrums

Characteristic peaks	Assigned wave numbers (cm^{-1})
-OH	3455
C-H	2918, 2850, 1467
S=O	1220, 1084, 835
Mo-S	590
H_2O	3455, 1654
M-O	589, 635

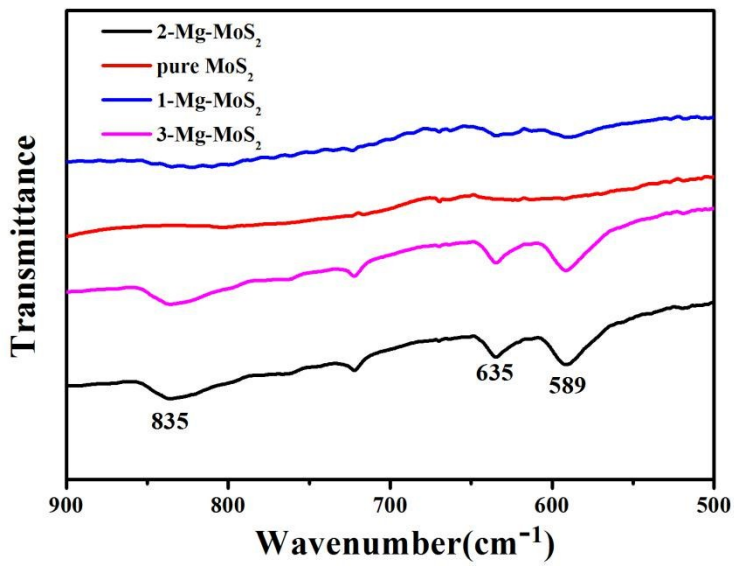

Fig. S3 FT-IR spectrums of 500-900 cm^{-1} of the pure MoS_2, 1-Mg-MoS_2, 2-Mg-MoS_2 and 3-Mg-MoS_2.

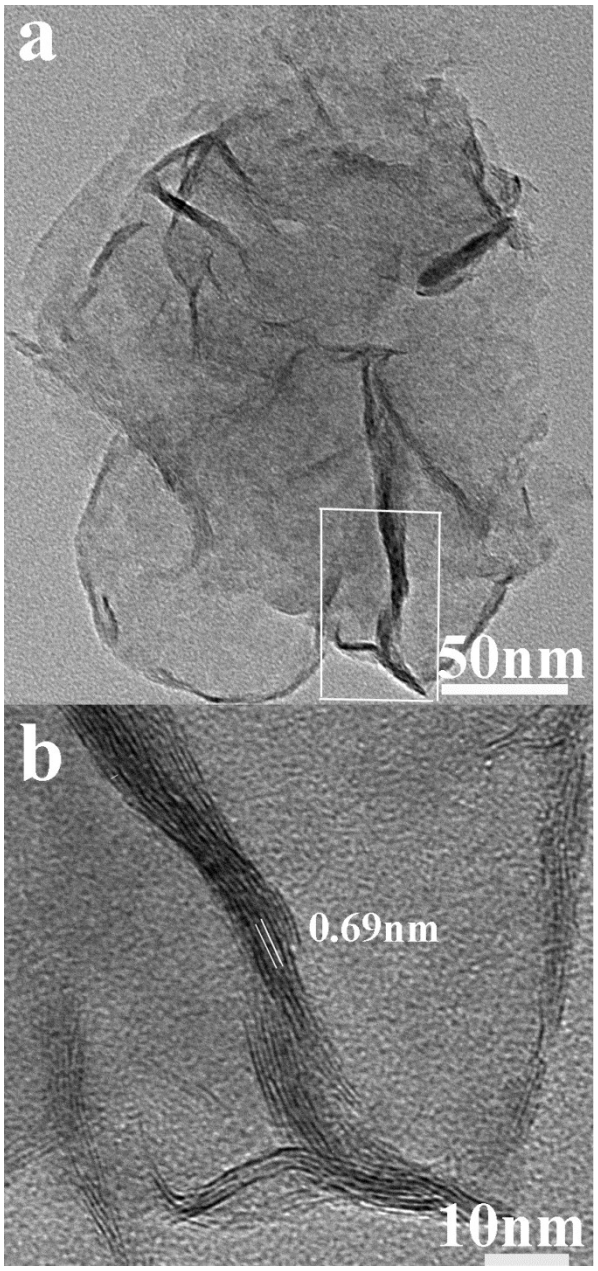

Fig. S4 TEM images of MoS_2 sample.

(a) TEM image, (b) HRTEM image of (a).

A typical lamellar structure of MoS_2 with interlayer spacing of 0.69 nm can be observed from the HRTEM image (Fig. S4b, the white square box in Fig. S4a), and the MoS_2 nanosheets mainly comprise more than 10 layers.

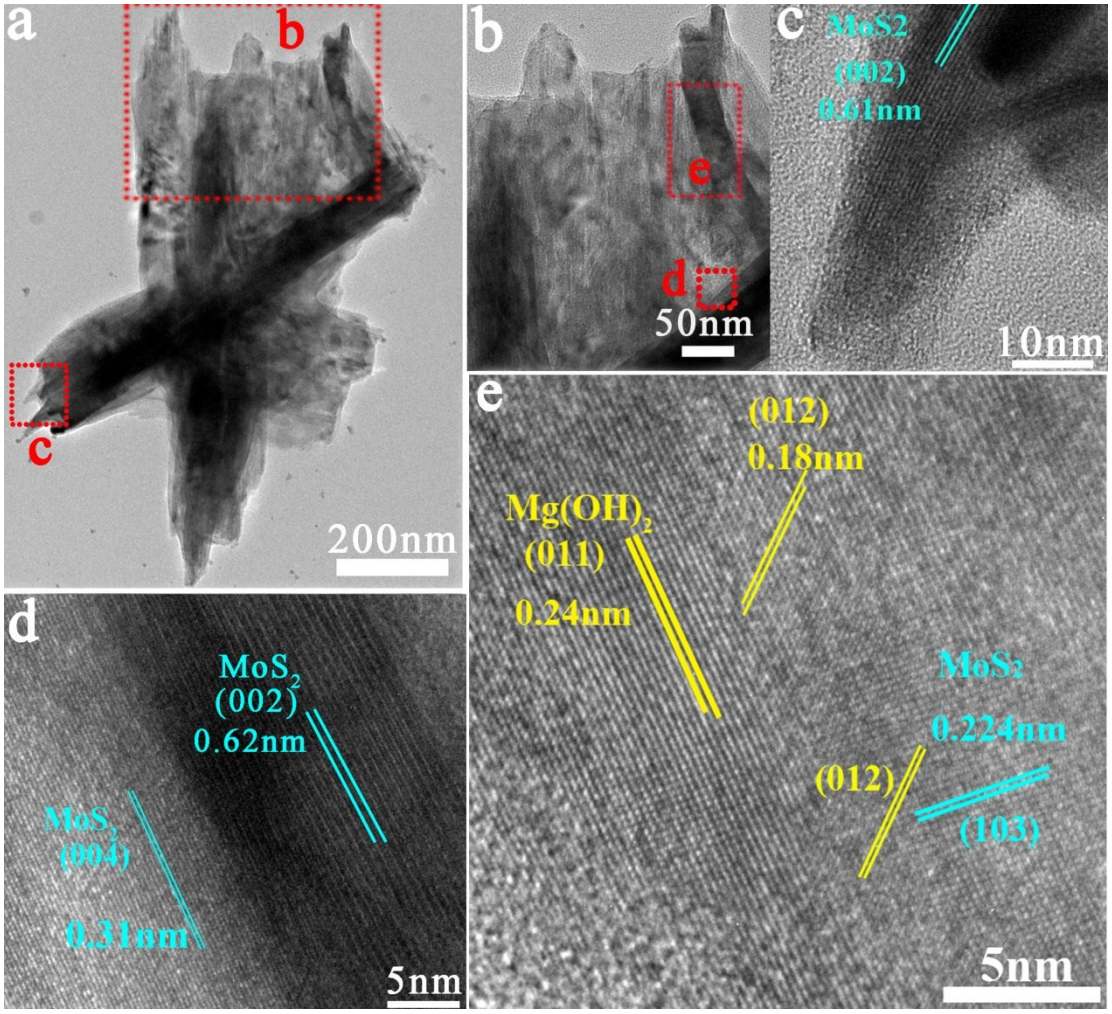

Fig. S5 TEM/HRTEM images of 3-Mg-MoS_2

(a) Low magnification TEM image of 3-Mg-MoS_2; (b) Enlarge TEM image of (a); (c) High magnification TEM (HRTEM) image of (a); (d), (e) HRTEM image of (b) (The sample contained 27 mol % MoS_2 in $Mg(OH)_2$@MoS_2 were named as 3-Mg-MoS_2).

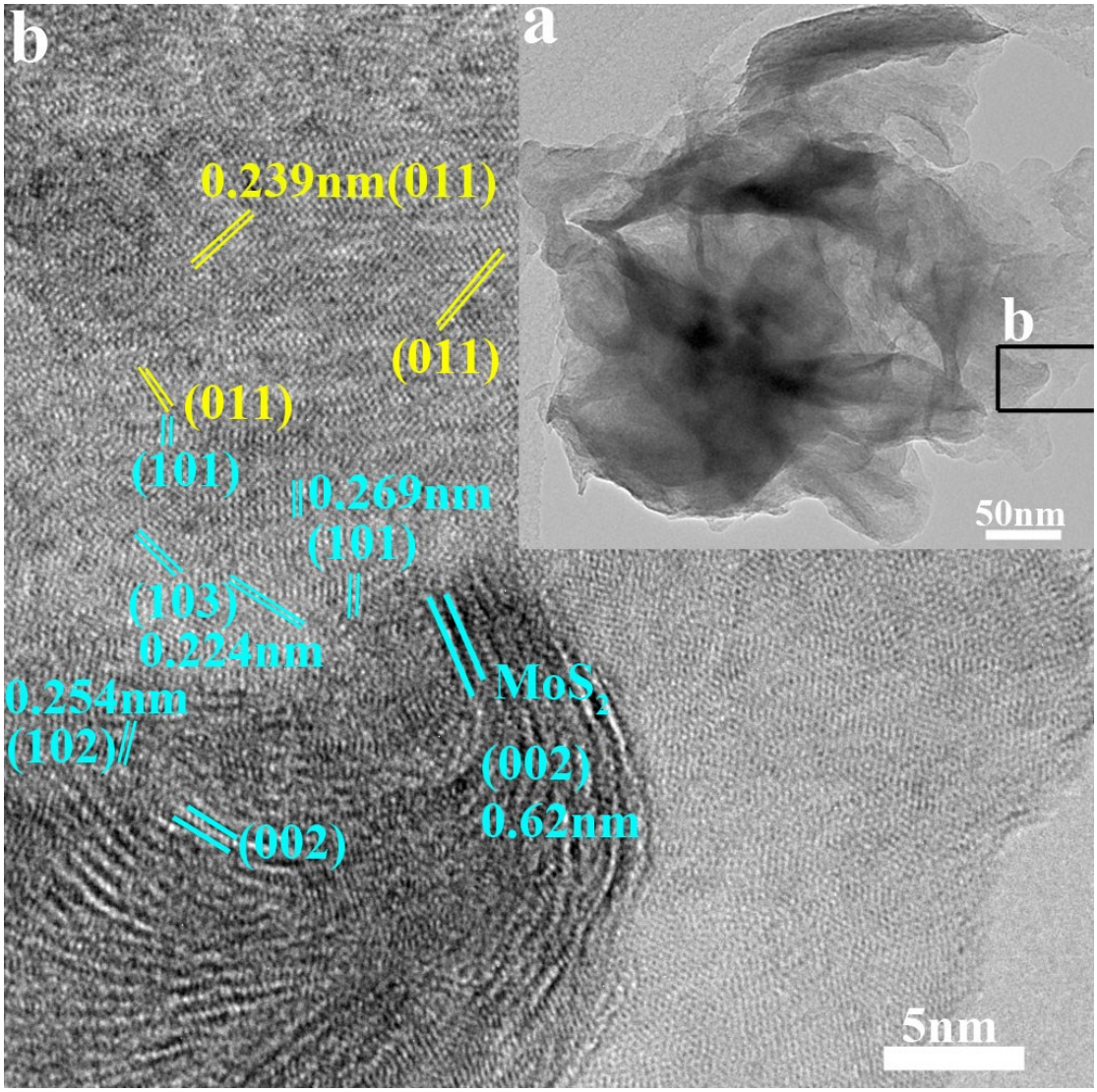

Fig. S6 TEM/HRTEM images of 1-Mg-MoS_2

(a) Low magnification TEM image of 1-Mg-MoS_2; (b) HRTEM image of (a).

(The sample contained 56.6 mol % MoS_2 in $Mg(OH)_2$@MoS_2 were named as 1-Mg-MoS_2).

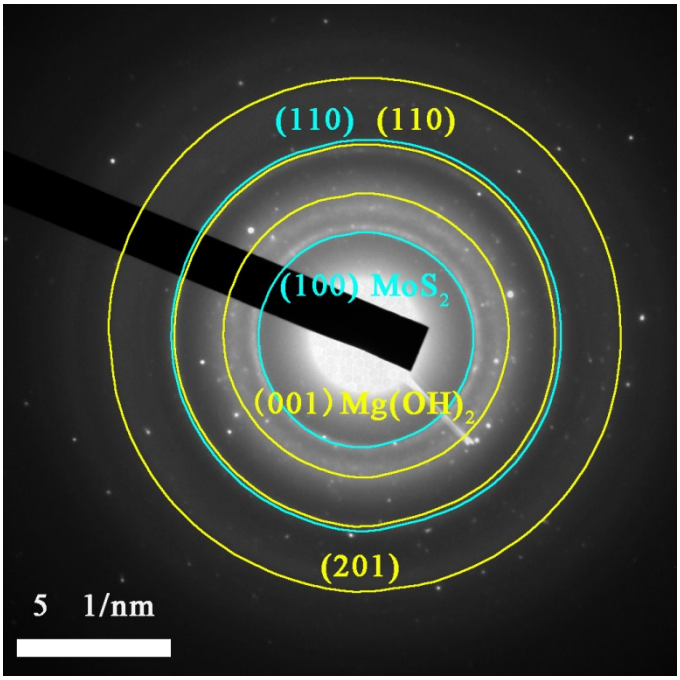

Fig. S7 The SAED pattern of 2-Mg-MoS_2.

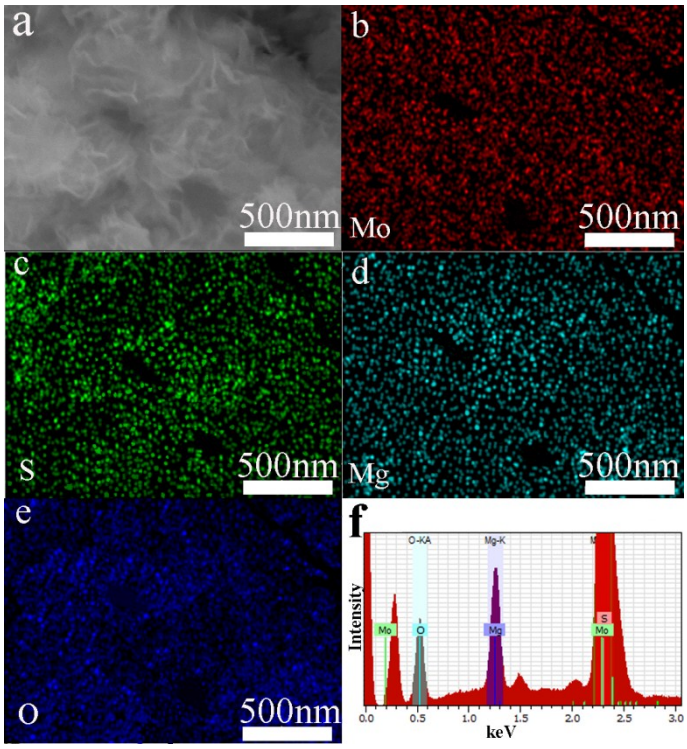

Fig. S8 SEM image/EDS mapping of 2-Mg-MoS_2 sample.

(a) SEM image; (b-e) Corresponding to Mo, S, Mg and O elemental mapping, respectively; (f) EDS spectra.

Table S2 The fitted impedance parameters of the pure MoS_2, 1-Mg-MoS_2, 2-Mg-MoS_2 and 3- Mg-MoS_2 samples.

Samples	R_Ω (Ω)	R_1 (Ω)	R_2 (Ω)	R_{ct} (Ω)
Pure MoS_2	74.03	2862	9537	4631
1-Mg-MoS_2	67.2	1284	1187	4009
2-Mg-MoS_2	13.64	2320	2250	1597
3-Mg-MoS_2	75.34	3.421×10^4	1675	2747

Table S3 The response results of the samples gas sensors to NO_x at room temperature.

Concentration	Response			
	2- Mg-MoS_2	pure MoS_2	1- Mg-MoS_2	3- Mg-MoS_2
100 ppm	4.73	1.44	2.0	2.26
50 ppm	3.39	1.25	1.82	2.08
20 ppm	3.13	1.23	1.5	1.41
5 ppm	2.65	1.22	1.58	1.36
3ppm	2.19	1.22	1.5	1.36
1ppm	1.65	1.11	1.23	1.33
0.5 ppm	1.54	1.1	1.18	1.22
0.3ppm	1.24	1.06	1.14	1.22
0.1ppm	1.19	1.04	1.14	1.13

Table S4 The response time of the samples gas sensors to NO_x at room temperature.

Concentration	Response time (s)			
	2- Mg-MoS_2	pure MoS_2	1- Mg-MoS_2	3- Mg-MoS_2
100 ppm	3.0	5.3	6.0	4.0
50 ppm	6.6	5.3	7.3	4.0
20 ppm	3.6	4.0	4.0	4.6
5 ppm	4.0	6.0	4.6	5.3
3ppm	4.0	6.6	4.6	11.7
1ppm	3.3	6.0	7.3	4.7
0.5ppm	3.3	8.7	7.0	11.0
0.3 ppm	4.7	8.7	8.0	11.0
0.1ppm	5.3	7.3	8.0	6.6

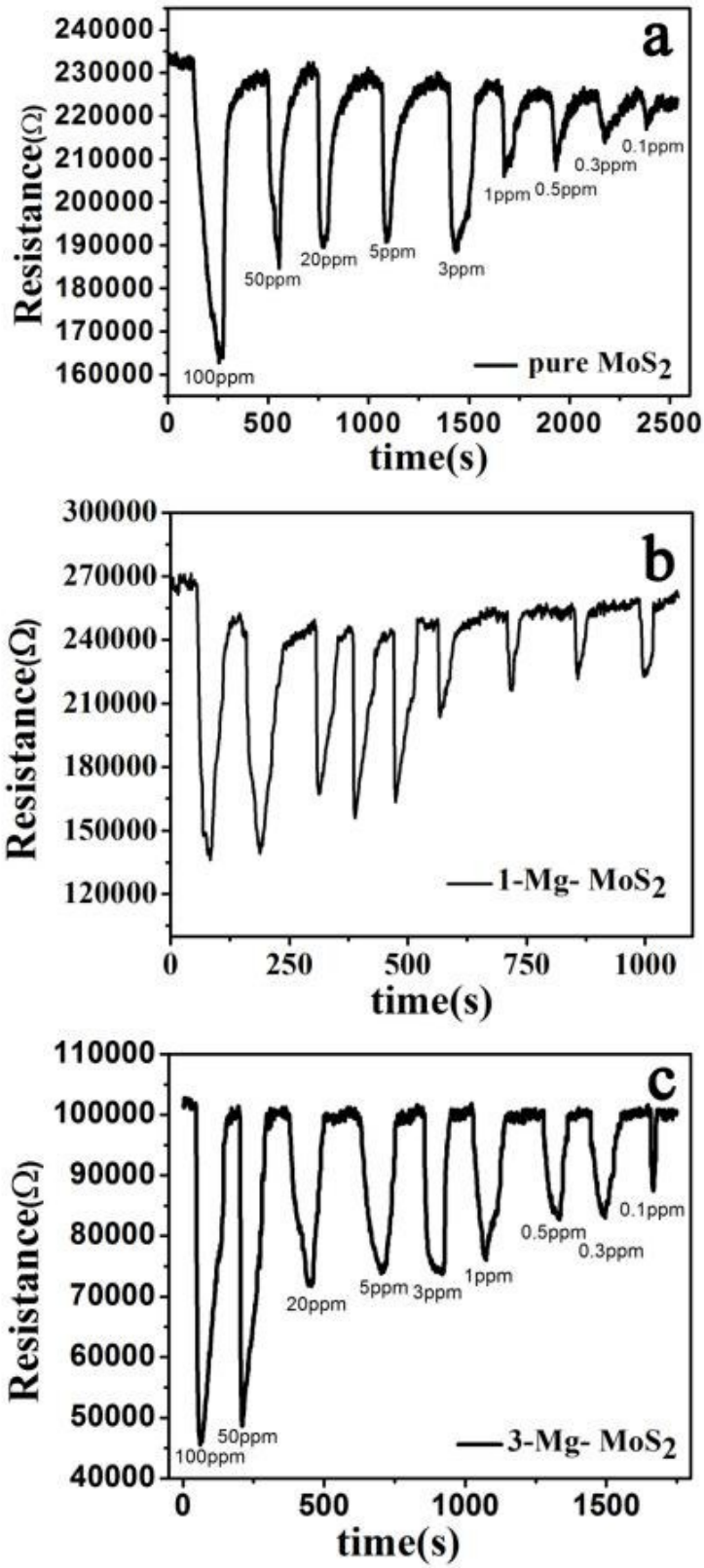

Fig. S9 Dynamical response transient of (a) pure MoS_2; (b) 1-Mg-MoS_2; (c) 3-Mg-MoS_2 to 0.1-100 ppm NO_x at room temperature.

Table S5 NO_x sensing performance of different chemiresistive gas sensors at room temperature

Materials	NO_x concentration (ppm)	Response time (s)	Recovery time (s)	Refs
MoS_2 FETs	0.8	120	400	2
MoS_2 -Pt NPs	0.5	>30min	>30min	3
$MoS_2/SiO_2/Si$	100	500	30min	4
MoS_2/SnO_2	10	408	162	5
$MoS_2/Mg(OH)_2$	0.1	5.3	60	This work

[1] R. D. Shannon. Acta Crystallographica Section A, 32(1976)751-767.

[2] H. Li , Z. Yin , Q. He, et al. small , 8(2012)63-67.

[3] Q. He, Z. Zeng, Z.Yin, et al. Small, , 8(201219)2994-2999.

[4] D. J. Late, Y. K. Huang, B. Liu, et al. Acs Nano, 7(2013)4879-4891.

[5] S. Cui , Z. Wen , X. Huang, et al. small , 11(2015)2305-2313.